

Explainable Incipient Fault Detection Systems for Photovoltaic Panels

Seshapalli Sairam, Seshadhri Srinivasan *Sr. Member, IEEE*, Giancarlo Marafioti *Sr. Member, IEEE*, B. Subathra, Geir Mathisen *Sr. Member, IEEE*, Korkut Bekiroglu *Member, IEEE*

Abstract—This paper presents an eXplainable Fault Detection and Diagnosis System (XFDDS) for incipient faults in PV panels. The XFDDS is a hybrid approach that combines the model-based and data-driven framework. Model-based FDD for PV panels lacks high fidelity models at low irradiance conditions for detecting incipient faults. To overcome this, a novel irradiance based three diode model (IB3DM) is proposed. It is a nine parameter model that provides higher accuracy even at low irradiance conditions, an important aspect for detecting incipient faults from noise. To exploit PV data, an extreme gradient boosting (XGBoost) is used due to its ability to detecting incipient faults. Lack of explainability, feature variability for sample instances, and false alarms are challenges with data-driven FDD methods. These shortcomings are overcome by hybridization of XGBoost and IB3DM, and using eXplainable Artificial Intelligence (XAI) techniques. To combine the XGBoost and IB3DM, a fault-signature metric is proposed that helps reducing false alarms and also trigger explanation on detecting incipient faults. To provide explainability, an eXplainable Artificial Intelligence (XAI) application is developed. It uses the local interpretable model-agnostic explanations (LIME) framework and provides explanations on classifier outputs for data instance. These explanations help field engineers/technicians for performing troubleshooting and maintenance operations. The proposed XFDDS is illustrated using experiments on different PV technologies and our results demonstrate the perceived benefits.

Index Terms—Explainable Artificial Intelligence (XAI) incipient fault, eXplainable Fault Detection and Diagnosis System (XFDDS), eXtreme Gradient Boosting (XGBoost).

I. INTRODUCTION

A. Motivation

EXPONENTIAL growth in photovoltaic (PV) deployments has raised interest in its reliable operation [1]. As PV panels are installed in harsh environments and subjected to varying weather conditions, they are prone to diverse faults (permanent, incipient, and intermittent) with different severity levels [2]. Such faults could diminish energy production, accelerate aging, and even cause fire hazards [3]. Therefore, detecting and locating faults early (at the incipient stage) is pivotal for the PV panel's reliable operations [4]. Detecting incipient faults challenging as the signatures are less evident due to low magnitude, and the problem accentuates at low irradiance conditions. Also, incipient faults are quite intermittent and show up for a short duration. Therefore, detecting them becomes more challenging. Nevertheless, incipient

faults could develop as a severe fault in the long-run if left undetected/unattended, leading to costly replacements and maintenance operations [5]. Consequently, detecting incipient faults has gained significant traction recently [6]. While fault-detection and diagnosis (FDD) systems are proven to improve PV system reliability [7], there are few challenges that need to be addressed for detecting incipient faults: (i) high fidelity PV models providing good accuracy at low irradiance conditions are required, (ii) existing FDD methods cannot reason their decisions to the field engineers/technicians, and (iii) difficult distinguishing between false alarms and incipient faults. Our objective in this paper is to propose an eXplainable Fault Detection and Diagnosis Systems (XFDDS) for incipient faults in PV panels that address challenges with FDD systems.

B. Literature Review

The FDD methods in the literature can be broadly discerned as being— model-based (MB), signal-based (SB), and data-driven (DD) [8]. The MB methods use PV panel models (set of nonlinear equations) followed by signal-analysis (e.g., correlation analysis) on the input-output data from the model to detect faults [9]. The single-diode model (SDM) [10], double-diode model (DDM) [11], and three-diode models (TDM) [12], [13] are widely used in FDD systems. While existing models provide good accuracy at high irradiance, their accuracy is less at low irradiance conditions. The SB methods use fault signatures from sensor data to detect faults [14]. Widely used SB methods are: statistical signal processing [15], I-V (current-voltage) characteristics analysis [16], power loss analysis [17] and, voltage and current measurements [18]. More recently, SB-FDD methods using two-stage support vector machines [19], multi-signal decomposition, and fuzzy inference systems [20] have also been proposed. The DD methods using labeled fault-data and artificial intelligence (AI) techniques have shown promise in improving detection accuracy due to their powerful model representation capabilities. The DD methods leverage historical labeled data and powerful models from AI techniques to perform multi-class regression or classification, which are quite important for detecting faults [21]. In the literature, FDD methods using AI models such as random forest [22], collaborative filtering [23], extreme gradient boosting [24], and such techniques have been proposing (see, [25] and references therein). Despite these advances, detecting incipient faults addressing the fundamental challenges of accuracy at low irradiance conditions, lack of explainability on decisions to field engineers/technicians, and distinguishing false alarms from incipient faults is rather unexplored in the literature to our best knowledge.

C. Contributions

This paper proposes an XFDDS for PV panels addressing challenges with FDD system. It is a hybrid method that combines model-based and data-driven approaches. To overcome accuracy challenges under low irradiance conditions

Seshapalli Sairam is with Dept. of Instrumentation and Control Engineering, Kalasalingam Academy for Research and Education, Krishnankoil, Srivilliputtur, India. e-mail : s.sairam@klu.ac.in

Seshadhri Srinivasan is with GE Corporate Research Center, Bangalore-560068. e-mail : seshadhri.srinivasan@ge.com

Giancarlo Marafioti is with SINTEF, Cybernetics. e-mail : giancarlo.marafioti@sintef.no

B. Subathra is with Dept. of Instrumentation and Control Engineering, Kalasalingam Academy for Research and Education, Krishnankoil, Srivilliputtur, India. e-mail : b.subathra@klu.ac.in

Geir Mathisen is with Norwegian University of Science and Technology Faculty of Engineering, Cybernetics. e-mail : geir.mathisen@ntnu.no

K. Bekiroglu is with the College of Engineering, SUNY Polytechnic Institute, Utica 13503, NY, USA. e-mail : korkut.bekiroglu@sunypoly.edu

and detect incipient faults, an irradiance based three diode model (IB3DM) proposed. The model uses irradiance and temperature in parameter computations inherently, thereby increasing its accuracy even at low irradiance conditions. For fault explainability and distinguishing false alarms from incipient faults, the IB3DM is combined with data-based approaches that perform multi-label classification. This paper uses the extreme gradient boosting (XGBoost) based multi-label classifier due to its suitability to detect incipient faults. As XGBoost cannot explain its decisions to the field technician/engineer, recently developed eXplainable AI (XAI) techniques are used. The XAI extends the capabilities of the AI techniques by providing explanations on decisions on individual data-instances [26], a key aspect in incipient fault detection. We show that these explanations are very useful for field engineers/technicians to understand the fault-causes and fault-type. The local interpretable model-agnostic explanations (LIME) approach is used [27] to provide the explanations. The main idea is to perturb the features and compute the importance and variable thresholds for being classified as faults on individual samples. Main contributions are:

1. A novel three diode model called the Irradiance Based Three Diode Model (IB3DM) which inherently captures the influences of solar irradiance and ambient temperature;
2. Design an XFDS leveraging the accuracy of IB3DM, XGBoost, and LIME;
3. Illustrate the IB3DM and XFDS using experiments and simulations on different PV technologies.

The paper is organized into five sections. The components of XFDDS is explained in Section II. The IB3DM for PV panel and its parameter computation is explained in Section III. The XFDDS methodology is presented in Section IV. Results are presented in Section V and conclusions are presented in Section VI.

II. EXPLAINABLE FAULT DETECTION AND DIAGNOSIS SYSTEM

The main challenges with existing FDD techniques are:

- (C1) Lack of high fidelity models capturing PV panel performance at low irradiance conditions;
- (C2) Existing FDD methods lack explanations to field engineers/technicians on why a particular sample was classified as faults and the variable thresholds on which this decision on a fault is made;
- (C3) Data-based models compute feature importance for a particular fault on the global data, whereas incipient faults are intermittent and there are inconsistencies within data instances as well;
- (C4) Data-based models cause false alarms due to misclassification.

The XFDDS proposed in our work addresses the challenges (C1)-(C4) and its schematic is shown in Fig. 1. Its main components are: climate service, IB3DM, fault-signature metric, the XGBoost classifier, XAI triggers, sample store and XAI application. The IB3DM uses the climate service (a web-application) to obtain solar irradiance and temperature for predicting the PV outputs (voltage, current, and power). Exploiting IB3DMs' model accuracy, a fault-signature metric is defined (see Section IV-B) which serves as a trigger for obtaining explanations from XAI application and such samples are stored in *sample store*, a local cache. The XGBoost based classifier is a combination of multiple classifiers, and

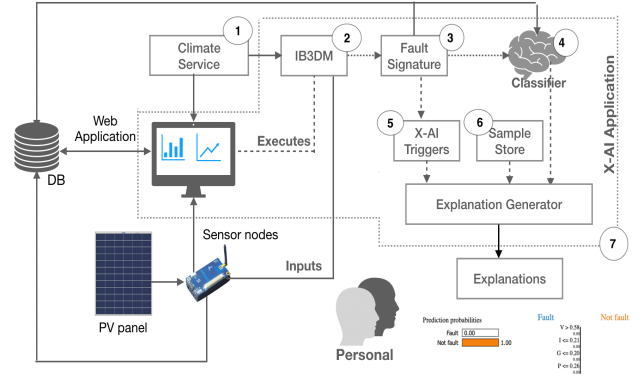


Fig. 1. Explainable fault detection system

regression tree (CART) ensemble created using boosting techniques [24]. The XGBoost is selected as the data-based model in our application, as it naturally fits the incipient fault-detection framework as detailed later. Two challenges with XGBoost are lack of explainability and false alarms [28]. Moreover, the feature importances for a particular fault are computed based on global data, contrary to this incipient faults are intermittent with data varying among fault samples (feature inconsistency problem). The particular of XAI application generate these explanations on a data-instances, which is very important for incipient faults. These explanations help the user to identify the fault types and variable thresholds based on which the fault was detected. In what follows the IB3DM model is first proposed and then the XFDDS approach is illustrated.

III. NOVEL IRRADIANCE-BASED THREE DIODE MODEL

Our model parameters depend on irradiance and module temperature and it addresses the challenge (C1). Therefore, we call our model irradiance-based three diode model (IB3DM). The IB3DM is an extension of the TDM proposed in [12], [13] wherein I_p , the light generated current depends on irradiance and module temperature. Further, in IB3DM, the ideality factors are not fixed; rather, they are obtained as a solution to an optimization problem by specifying bounds ($[0, 2]$). This is a deviation from existing works in three diode models where higher ideality factors are used leading to low fill-factor that could be achieved only in industrial-grade panels. This makes existing TDM unsuitable for residential PV panels.

A. Equivalent Circuit and Model Parameters

Our idea is to propose a three diode model that accurately captures the PV cells' performance even under low irradiance conditions.

Remark 1. In IB3DM, the source current is modelled as a dependent current source that is a function of irradiance and module temperature, denoted by $I_p(G, T)$. The photo-generated current has two parts; the first part which is a premultiplier is linearly dependent on the irradiance and acts as a scaling factor for the second part that depends on panel temperature.

Suppose the nominal phase current is denoted by $I_{p,n}$, then the dependence on phase current on the irradiance is given by,

$$I_p(G, T) = \left(\frac{G}{G_{STC}} \right) \left(I_{p,n} + K_I \times (T - T_r) \right) \quad (1)$$

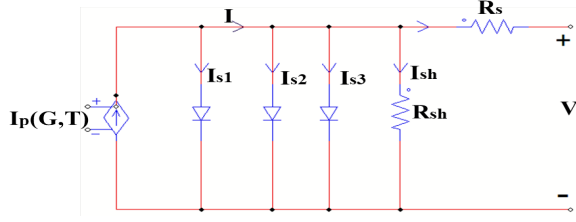


Fig. 2. Equivalent circuit of IB3DM.

where K_I is a constant computed from data-sheets. The source current is in parallel to three diodes with a series resistance R_s and shunt resistance R_{sh} , as shown in Fig. 2. With this modification, the current source is a function of irradiance and module temperature. From the equivalent circuit, the output current is given by

$$I = I_P - I_{I1} - I_{I2} - I_{I3} - I_{sh} \quad (2)$$

Similarly, current through the shunt resistance R_{sh} in Fig. 2 is,

$$I_{sh} = \frac{V + IR_s}{R_{sh}} \quad (3)$$

The diode saturation currents can be calculated as:

$$I_{01} = \frac{I_S + K_I \times (T - T_r)}{\exp\left(\frac{V_{OC} + K_V \times (T - T_r)}{V_t \times n_{01}}\right) - 1}, \quad (4)$$

$$I_{02} = \frac{I_S + K_I \times (T - T_r)}{\exp\left(\frac{V_{OC} + K_V \times (T - T_r)}{V_t \times n_{02}}\right) - 1}, \quad (5)$$

$$I_{03} = \frac{I_S + K_I \times (T - T_r)}{\exp\left(\frac{V_{OC} + K_V \times (T - T_r)}{V_t \times n_{03}}\right) - 1}, \quad (6)$$

The saturation currents strongly depends on the temperature as indicated by equations (4)-(6). Note that the coefficient K_V is from the manufacturers' data-sheet and used to compute I-V curve for different temperatures as seen the equations (4)-(6). The junction thermal voltage is given by,

$$V_t = \frac{N_s k T}{q}. \quad (7)$$

Combining equations (1)-(7), one can obtain the equations relating the output current, output voltage, and model parameters for the IB3DM:

$$\begin{aligned} I = & I_P - I_{01} \left(\exp\left(\frac{V + IR_s}{n_{01} V_t}\right) - 1 \right) \\ & - I_{02} \left(\exp\left(\frac{V + IR_s}{n_{02} V_t}\right) - 1 \right) \\ & - I_{03} \left(\exp\left(\frac{V + IR_s}{n_{03} V_t}\right) - 1 \right) - \frac{V + IR_s}{R_{sh}}, \end{aligned} \quad (8)$$

where n_{01} , n_{02} , and n_{03} are diode ideality factors. Consequently, the IB3DM has nine parameters given by $\mathcal{P}_{IB3DM} = \{I_P, I_{I1}, I_{I2}, I_{I3}, R_s, R_{sh}, n_{01}, n_{02}, n_{03}\}$ which should be obtained from I-V curve data. Next step is to compute the model parameters and an optimization based approach is proposed as detailed in the next section.

B. The IB3DM Parameter Computation

To compute the IB3DMs' model parameters, first the I_P is calculated using G and T from equation (1). Next, we define the objective function as the root mean square error between the experimental V-I and the estimated model is given by,

$$\begin{aligned} f_m(V, I, \mathcal{P}) = & I - I_P + I_{01} \left(\exp\left(\frac{V + IR_s}{n_{01} V_t}\right) - 1 \right) \\ & + I_{02} \left(\exp\left(\frac{V + IR_s}{n_{02} V_t}\right) - 1 \right) \\ & + I_{03} \left(\exp\left(\frac{V + IR_s}{n_{03} V_t}\right) - 1 \right) + \frac{V + IR_s}{R_{sh}} \end{aligned} \quad (9)$$

It measures the difference between experimental I-V curve data and the one calculated using the model, i.e., $f_m(V, I, \mathcal{P}) = I_{measured} - I_{calculated}$ with V varying over the operating range. To compute the model parameters, we utilized the root mean square error (RMSE) as a metric denoted by, $\mathcal{J} = \sqrt{\frac{1}{N_e} \sum_{i=1}^{N_e} f_m(V, I, \mathcal{P})^2}$. The parameter computation problem is modelled as an optimization problem given by,

$$\begin{aligned} \min_{\mathcal{P}_{IB3DM}} \quad & \mathcal{J} \\ \text{s.t.} \quad & (2) - (8) \end{aligned} \quad (10)$$

Clearly, (10) is nonlinear and non-convex that is computationally complex to solve using conventional optimization techniques. Usually meta-heuristic approaches are used for computations for this type of optimization problems [29]. Our analysis utilizes five different meta-heuristic algorithms that are explained in results section.

IV. EXPLAINABLE FAULT DETECTION AND DIAGNOSIS METHODOLOGY

A. Extreme Gradient Boosting for Fault Classification

Gradient boosting decision tree is a powerful machine learning algorithm wherein multiple weak learner ensemble form a strong learner [30]. The XGBoost main idea is that the training set in the current instance is related to the learning results from previous learning, and the weights on data-samples are adjusted on each sample in each iteration. These features naturally fits the incipient fault-detection scenario as labeled fault-data are available sequentially, and weight adaptation in each sample increases model accuracy. Furthermore, in XGBoost the current decision tree (leaf) is fitted based on the residuals from the previous trees and it uses the gradient boosting principle wherein new decision trees are constructed to correlate to the negative gradient of the loss-function. A detailed description of XGBoost could be found in [31], [32].

This investigation uses XGBoost for detecting two incipient faults: (i) line-to-line (LL) fault which denotes short-circuit within the string or on multiple PV strings and (ii) partial shading. Two different classification cases are considered: binary and multi-class classification. In binary classification, labeled data about whether a given sample is faulty or healthy operating condition is predicted without considering the fault-type (LL or partial shading), whereas in multi-class fault classification, the fault-type are also included as additional class.

In binary classification, voltage, current, irradiance, and power are the inputs and a binary variable modelling the

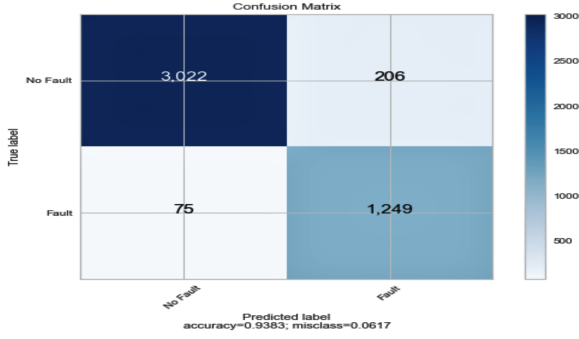


Fig. 3. Confusion Matrix for Binary Classification

sample to be faulty/healthy is the output. Dichotomous search optimization was used for tuning hyper-parameters that resulted in 100 learners. During training, the classifier showed 93-95% accuracy, and validation had 86-93% accuracy. The confusion matrix for the binary classifier is shown in Fig. 3. One can see that the classifier performs extremely well for binary classification.

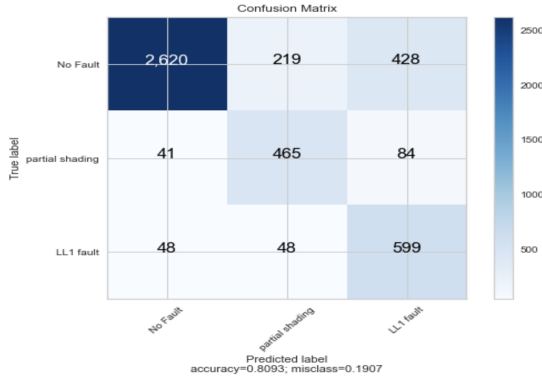


Fig. 4. Confusion Matrix for Multi-Class Classification

In multi-class classification, additional labels on the fault type (LL), or partial shading) is added to the data-set. Then the XGBoost classifier is trained to identify the fault label. The XGBoost hyper parameters was optimized using dichotomous search and it had 130 learners. During the training, the classifier showed 88-92% accuracy, and 78-82% during validation. Confusion matrix for the multi-class classification during validation is shown in Fig. 4. While its accuracy is reasonable, the challenges (C2)-(C4) are not addressed by XGBoost.

B. Explainable Fault Detection

To provide local explanations and address challenges (C2)-(C4), the data-driven approach is first fused with model-based approach by proposing a fault-signature metric (FSM) given by,

$$\sigma(G, P) = \gamma(G) \exp\left(\frac{-\|G - G_s\|_{\ell_2}}{\Sigma_G}\right)^{-1} \times \exp\left(\frac{-\|P - \hat{P}\|_{\ell_2}}{\Sigma_P}\right) \quad (11)$$

where $\gamma(G)$, Σ_G , and Σ_P are the scaling factor as a function of irradiance, variances in the actual solar irradiance, and power generated by the solar panel, respectively. Also, $\|\cdot\|_{\ell_2}$ represents ℓ_2 norm. \hat{P} is the estimated power computed by the

IB3DM, and the signature computes the deviations in power. The fault-signature metric serves two purposes: (i) it weights low variability at low irradiance conditions higher than at high irradiance conditions helps overcoming noise and preventing false alarms and (ii) triggers for explanations on detecting an incipient fault by using thresholds on fault-signature metric.

The XFDDS uses FSM to eliminate false alarms by comparing it with results of the XGBoost. Second, event triggers for fault explanations are generated using FSM. Once the FSM exceeds a known threshold, explanations are asked from the XAI application and such samples are stored in sample store.

On receiving triggers, the XAI application is activated that uses the local interpretable model-agnostic explanations (LIME) [27] framework. It utilizes surrogate modelling wherein the model is considered a black-box, and the features are perturbed to find feature importance on a particular sample. The data instance is perturbed, and samples are generated from the data-set distribution, which is weighted based on their distances from the current point. Then feature selection is applied to keep the relevant variables, and the linear model is trained on the weighted data-set automatically within the algorithm. Once trained, the model explains to the user about the variables and their thresholds that made the model decide a particular sample instance as a fault/normal operation. This is quite useful in detecting incipient faults as they are intermittent and occur for a few fault-samples.

While the core of XFDS is still the XGBoost, the XAI extracts explanations on why a particular sample was classified as being faulty/healthy. Further, thresholds on variables that helped make these decisions are also provided, which is quite useful in detecting even the fault type. For example, a LL fault is characterized by high voltage but a lower current and power. As power drops due to circulating currents are very hard to predict. Moreover, intermittent LL faults are difficult to catch FDDS. However, with XAI could reason out incipient LL faults.



Fig. 5. Experimental setup using a PV module.

V. RESULTS

The proposed XFDDS could be implemented on simple hardware as illustrated in this section. In our experiments, the fault-detection is implemented by interfacing embedded hardware with computer. However, the computer could be replaced with any system-on-chip (SoC) with limited computing power. The computer interfaces to the web application directly and obtains the weather data. The weather station recordings are ported as a comma-separated variable. The ATmega 328P processor is used as the data-acquisition unit, which interfaces to the computer through the software application and receives the measurements from sensors. Measurements

were obtained from the current sensor (INA169), temperature sensor (DS18B20), and voltage sensor (F031-06), respectively. The data was transmitted to the computer using the UART (Universal Asynchronous Receiver/Transmitter), a serial communication mode to PLX-DAQ and the measurements are stored in a data-base for further processing. Temperature sensor Maxim IC DS 18B20 is a 1-wire digital temperature sensor that reports temperature in Celsius with 9-12 bit precision and has a working range of -55 to 125°C . A rheostat is used as the load, and the experiments are conducted at International Research Center, Kalasalingam University, India. Experiments with PV panel, sensors interfaced with computers, and Python was used to implement the fault-detection scheme (see Fig. 5).

A. The IB3DM Model Parameter Estimation

As stated earlier, the IB3DM parameter computation requires solving a nonlinear and non-convex optimization problem in (10). To overcome computational difficulties, five different meta-heuristic algorithms are used: (i) firefly, (ii) particle swarm optimization (PSO), (iii) teaching-learning based optimization (TLBO), (iv) biogeography based optimization (BBO), and (v) shuffled frog leaping algorithm (SFLA) to estimate the model parameters of the IB3DM.

The parameter is computed for two different PV technologies: monocrystalline (STM5-20/36) at 1000 W m^{-2} at 33° and polycrystalline (Solartech SPM-020P-R) with 1000 W m^{-2} at 45° with each panel having 36 cells in series.

The IB3DM parameters computed for a monocrystalline panel for the SDM, DDM, CD3DM, and IB3DM with the five meta-heuristic algorithms is shown in Tab. I. The RMSE value (\mathcal{J}) are shown in Tab. I. One can observe that IB3DM offers better accuracy than existing models as evinced by their low RMSE values. In addition, fire-fly algorithm provides better estimates of the I-V curves.

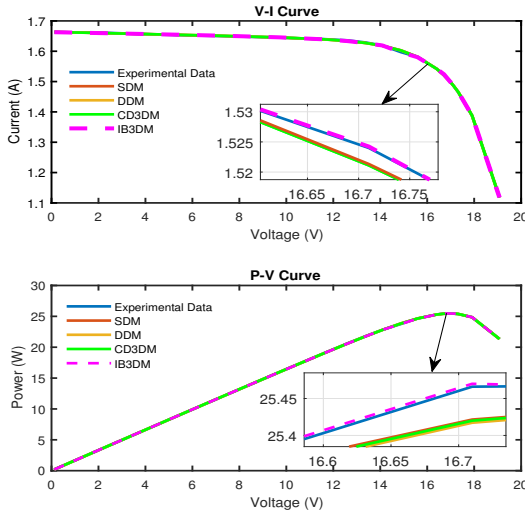


Fig. 6. (a) V-I Curve of the SDM, DDM, C3DM versus IB3DM, (b) P-V Curve of SDM, DDM, C3DM, and IB3DM (Monocrystalline).

A comparison of the I-V and P-V curves with model parameters computed by the firefly algorithm for the different PV models: SDM, DDM, CD3DM, and IB3DM is shown in Fig. 6. The accuracy provided by IB3DM at MPP is also shown in the zoomed portion. Similarly, accuracy is also high at low and high irradiance conditions as well.

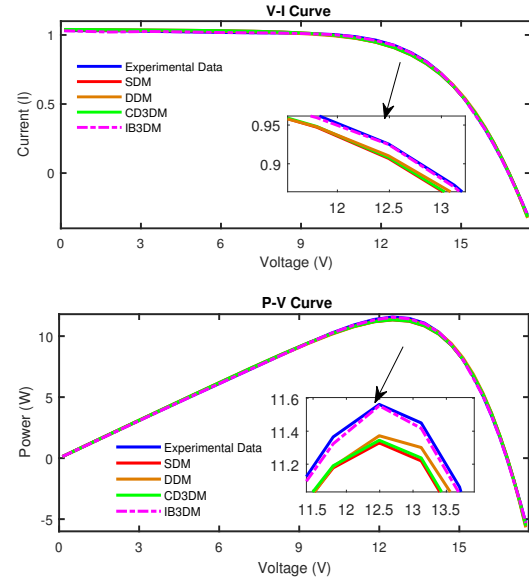


Fig. 7. (a) V-I Curve of the SDM, DDM, C3DM versus IB3DM, (b) P-V Curve of SDM, DDM, C3DM, and IB3DM (Polycrystalline PV panel)

The IB3DM model parameters and its comparison with other PV models for poly-crystalline panel (SPM-020P-R) is shown in Tab. II. The low RMSE values are indicative of the accuracy provided by IB3DM. Further, firefly algorithm provides the best model parameters compared with other meta-heuristic techniques. Similarly, the I-V and P-V curves for the different diode model is shown in Fig. 7. This results shows the model accuracy across irradiance levels. These results demonstrate the IB3DMs' ability to provide model accuracy across different irradiance levels and PV technologies.

B. Explainable Incipient Fault Detection

Having computed the model parameters, the next step is to fuse IB3DM with XAI to implement the XFDDS. First, we show the ability of IB3DM to detect faults and then extensions to providing explanations are presented. Two studies used to illustrate XFDDS capabilities:

- (i) Single-cell in a module is partially shaded in a PV panel consisting of 36 cells in series;
- (ii) Most cells in a array are partially shaded (8 among 36) in different proportions (10-90%).

These two cases cover most scenarios envisaged during the PV panel operations and the incipient fault was created artificially for the study.

C. Case Study 1

This study considers fault in polycrystalline panel (Solartech SPM-020P-R) using IB3DM. To illustrate IB3DM ability to detect fault, the V-I and P-V curves are computed at different irradiance levels ($0-1000\text{ W m}^{-2}$, 800 W m^{-2} , and 450 W m^{-2}). The I-V and P-V curves are shown in Fig.9 (a) and (b), respectively. One can see that the IB3DM predictions exactly coincide with experimental V-I and P-V curves, whereas model errors are high with other models. Furthermore, slope of the PV curves at lower voltages are indicative of the incipient fault and this is illustrated from fault

Table I: Comparison of meta-heuristic algorithms for computing the model parameters of the Monocrystalline panels

Model	Algorithm	$I_P(A)$	$I_{01}(A)$	$I_{02}(A)$	$I_{03}(A)$	n_1	n_2	n_3	$R_s(\Omega)$	$R_{sh}(\Omega)$	K	$RMSE$
SDM	Firefly	1.6644	1.55E-06	-	-	1.94	-	-	0.176	752.29	-	0.012245
	PSO	1.6626	2.87E-06	-	-	1.87	-	-	0.3917	599.78	-	0.060392
	TLBO	1.6634	2.86E-06	-	-	1.67	-	-	0.4255	598.55	-	0.042516
	BBO	1.6605	9.08E-07	-	-	1.99	-	-	0.6372	642.66	-	0.065356
	SFLA	1.663	6.02E-06	-	-	1.96	-	-	0.2385	690.27	-	0.083196
DDM	Firefly	1.6645	1.71E-06	3.01E-12	-	1.85	1.72	-	0.2396	739.49	-	0.010945
	PSO	1.7029	3.08E-05	6.24E-05	-	1.64	1.55	-	0.1263	606.28	-	0.052871
	TLBO	1.6638	1.14E-10	5.21E-06	-	1.52	1.91	-	0.5215	695.23	-	0.042925
	BBO	1.7029	3.08E-05	6.24E-05	-	1.94	1.55	-	0.3263	606.28	-	0.085258
	SFLA	1.6613	5.66E-06	2.24E-08	-	1.76	1.89	-	0.2199	673.52	-	0.092876
CD3DM	Firefly	1.6645	2.71E-06	3.01E-12	1.08E-05	1.72	1.57	1.47	0.296	739.49	0.0092	0.004852
	PSO	1.7029	1.08E-05	2.24E-05	1.72E-05	1.52	1.22	1.42	0.2263	656.28	0.0272	0.018471
	TLBO	1.6638	2.24E-10	3.31E-06	4.24E-08	1.49	1.19	1.24	0.3215	595.23	0.0231	0.009229
	BBO	1.7029	1.98E-05	2.41E-05	3.23E-08	1.76	1.28	1.62	0.2363	596.28	0.0185	0.024528
	SFLA	1.6613	2.66E-06	5.24E-08	4.76E-06	1.62	1.24	1.32	0.2699	473.52	0.0289	0.050476
IB3DM	Firefly	1.6633	2.93E-06	5.10E-15	1.54E-07	1.35	1.46	1.24	0.0917	804.43	-	0.005463
	PSO	1.7133	6.88E-04	1.80E-10	1.63E-09	1.02	1.09	1.14	0.3618	477.24	-	0.007824
	TLBO	1.6622	1.89E-08	8.67E-08	1.19E-05	1.08	1.06	1.15	0.3917	761.51	-	0.005936
	BBO	1.6683	8.52E-06	4.13E-06	2.85E-04	1.03	1.12	1.39	0.2511	570.46	-	0.008193
	SFLA	1.6683	8.52E-06	4.13E-06	2.85E-04	1.13	1.18	1.29	0.3511	570.46	-	0.008262

Table II: Comparison of meta-heuristic algorithms for computing the model parameters of the Polycrystalline panel

Model	Algorithm	$I_P(A)$	$I_{01}(A)$	$I_{02}(A)$	$I_{03}(A)$	n_1	n_2	n_3	$R_s(\Omega)$	$R_{sh}(\Omega)$	K	$RMSE$
SDM	Firefly	1.047	4.43E-05	-	-	1.85	-	-	1.7763	612.53	-	0.030324
	PSO	1.0458	5.86E-05	-	-	1.96	-	-	1.7286	680.97	-	0.549642
	TLBO	1.0345	1.91E-05	-	-	1.86	-	-	1.9521	684.96	-	0.495359
	BBO	1.0343	1.43E-04	-	-	1.97	-	-	1.4589	653.48	-	0.576291
	SFLA	1.0466	1.31E-04	-	-	1.98	-	-	1.5583	699.79	-	0.762183
DDM	Firefly	1.0435	5.15E-05	6.03E-13	-	1.83	1.65	-	1.7621	611.84	-	0.027368
	PSO	1.0676	7.88E-05	6.03E-08	-	1.91	1.71	-	1.7272	591.83	-	0.389554
	TLBO	1.0323	2.14E-05	5.37E-06	-	1.79	1.69	-	1.1532	692.98	-	0.069885
	BBO	1.0881	1.55E-05	6.62E-04	-	1.93	1.79	-	1.0243	641.61	-	0.401265
	SFLA	1.0971	1.67E-04	3.53E-05	-	1.95	1.82	-	1.0004	358.15	-	0.495239
CD3DM	Firefly	1.0745	1.62E-06	1.92E-12	3.28E-05	1.62	1.48	1.28	1.0235	798.25	0.0052	0.011619
	PSO	1.0929	6.54E-05	1.54E-05	1.92E-05	1.85	1.62	1.59	1.0563	696.28	0.0237	0.387132
	TLBO	1.6538	1.52E-10	2.26E-06	5.42E-08	1.68	1.34	1.45	1.5235	495.23	0.0259	0.065293
	BBO	1.0029	1.98E-05	2.41E-05	3.23E-08	1.89	1.67	1.62	1.0063	606.28	0.0262	0.537698
	SFLA	1.0513	3.66E-08	3.24E-06	3.76E-09	1.91	1.73	1.71	1.0039	623.52	0.0325	0.553676
IB3DM	Firefly	1.047	2.27E-10	2.39E-04	2.03E-12	1.42	1.37	1.06	1.0954	729.53	-	0.004856
	PSO	1.049	8.33E-06	4.64E-04	3.70E-12	1.66	1.54	1.23	1.9449	693.99	-	0.006806
	TLBO	1.042	3.32E-06	1.06E-04	1.17E-05	1.53	1.45	1.03	1.2107	671.01	-	0.005077
	BBO	1.039	1.43E-05	4.11E-05	4.67E-05	1.72	1.62	1.35	1.5124	697.74	-	0.007493
	SFLA	1.045	2.63E-05	2.92E-07	2.26E-05	1.79	1.67	1.49	1.9119	691.77	-	0.007994

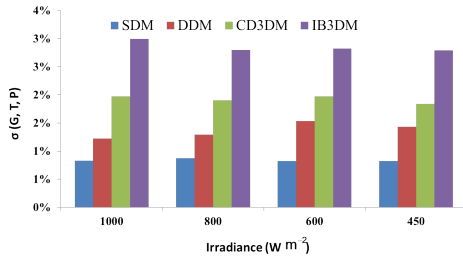


Fig. 8. Fault signature for different irradiance.

signatures at low irradiance conditions (see, Fig. 8). Using this fault-signature metric, the XFDDs could avoid false alarms (false positives). This results illustrates the ability of IB3DM to detect partial shading in single cell and avoid false alarms raised by XGBoost classifier. Moreover, detecting incipient faults is challenging with IB3DM alone.

D. Case Study 2

The IB3DMs' ability to detect faults in *monocrystalline* array with partial shading of different magnitudes across PV panel is illustrated. Variations in power curves with the SDM, DDM, CD3DM, and IB3DM for irradiance levels (0-1000

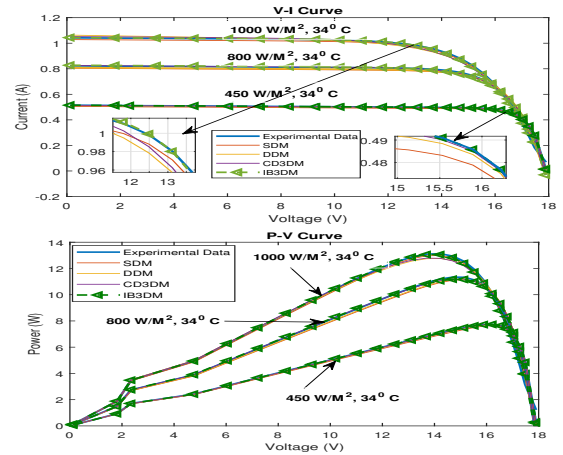


Fig. 9. (a) V-I Curve for different irradiance, and (b) P-V Curve for different irradiance (polycrystalline).

$W m^{-2}$) are considered. Due to partial shading, the voltage reduction is not severe, whereas the current reduction is quite high which gets reflected in the power curve as well. This is illustrated in Fig. 10 and is indicative of a fault. This is observed in fault-signature metric as well. These findings when combined with XGBoost based classifier could reduce mis-

classification and false alarms.

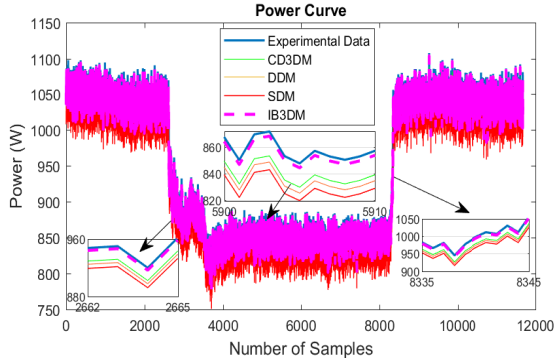


Fig. 10. Power curve for Partial shading condition for PV panel

There are two shortcomings with just IB3DM based detection. It requires enough significant sample averages to detect incipient faults which is seldom possible due to their intermittent nature. Next, they cannot identify fault types nor provide explanations.

E. XFDDS for Incipient Faults

The XFDDS is implemented on two different XGBoost implementations, binary and multi-class classification. The XGBoost leverages data and averts false alarms by using IB3DM fault-signature metric. In this study, the monocrystalline panel string consisting of 56 panels at the International Research Center, Kalasalingam University, is used as the pilot to demonstrate the XFDDS. In binary classification, the XGBoost classifies whether a given test sample is faulty/healthy. This is compared with the fault-signature metric outcomes. Using a threshold on FSM and based on XGBoost classifier outcomes, explanations are triggered.

In our study, the partial shading fault was created artificially by covering panels with papers. A sampling time of 1 s and the fault is created at 2400 samples for a duration of 32 minutes. These samples are passed to the IB3DM, which detects the presence of incipient fault through its fault signature. This triggers the XAI application to generate explanations. The explanations for partial shading faults are shown in Fig. 11. The explanations are very intuitive for detecting incipient partial shading fault. As the explanation shows that the irradiance ($G \geq 896$) and the voltage ($V \geq 141.29$ V), but the current (≤ 9.77 A) and the power magnitudes (≤ 1354 W) are low. This is indicative of a partial shading fault for the field engineer.

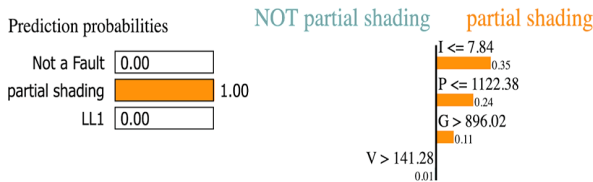


Fig. 11. Partial shading fault

Similarly, the LL fault was created by shorting out the lines within a single string for a short duration. The IB3DM generates fault-signature of the power curve, which triggered the explanations that are shown in Fig. 12 which is explaining that current values are less than 7.44A and power values lesser

than 1112.52 W while the voltage is greater than 141.29 V helps the XFDDS decide that there is a LL fault.

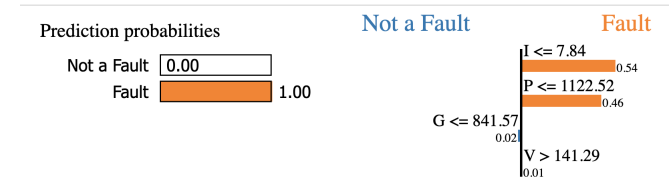


Fig. 12. Line-to-Line Fault

Explanations on a sample which was false positive detected by XGBoost and explanations provided by the XAI is shown in Fig.13. Here the decision was based on the current value, which was less than 7.84 A. However, the power level greater than 1112.89 W shows that this is not a fault. This way, false positives could be avoided by explanations, and this denotes an intermittent behaviour of the load to the field engineer.

Next, the XFDDS was applied to multi-class classification problem. In this case, the fault-labels were given as input as well. The IB3DM was used to trigger explanations using thresholds on fault-signature metric. The explanations for the incipient LL fault is shown in Fig. 14. In this case the XGBoost identifies the LL fault and the causes are illustrated by current (≤ 7.84 A) and power (less than 1122.38 W).

The explanations for partial shading faults are shown in Fig. 15. The explanations are very intuitive as the current and power are less than a threshold, whereas the irradiance is greater than 896 W m^{-2} . The fault could be easily understood by the field technicians. Furthermore, the threshold values are explained to the field engineers on current, power, irradiance, and voltage. This result also shows that the explanations and the thresholds are oblivious to the classification label, i.e., binary or multi-class.

VI. CONCLUSIONS

This paper presented an explainable fault-detection and diagnosis system (XFDDS) for detecting incipient faults in PV panels. Its main components were: irradiance based three diode model and explainable artificial intelligence (XAI) application. The IB3DM used irradiance and temperature to compute its model parameters, thereby increasing its accuracy even at low irradiation conditions. The model parameters

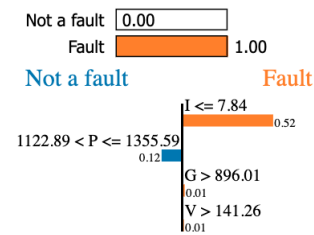


Fig. 13. Line-to-Line Fault Explanation

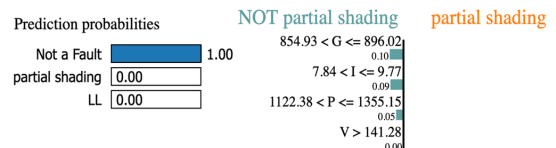


Fig. 14. Explanations for LL-fault Multi-Label Classification

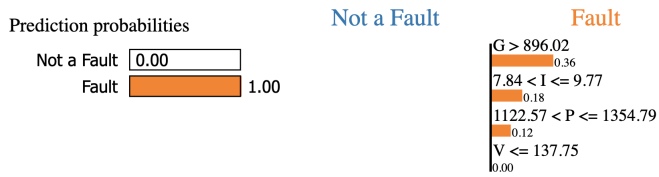


Fig. 15. Explanations for Partial Shading Faults

were computed solving a non-convex constrained optimization problem with five different meta-heuristic approaches. Our results demonstrated the model fidelity of the IB3DM even at low irradiance conditions. To exploit the aggregated data from PV panels, an extreme gradient boosting (XGBoost) based classifier was used and it had two shortcomings: false alarms and lack of explainability. False alarms were reduced by combining IB3DM with XGBoost classifier by proposing a fault-signature metric (FSM). Explanations were provided by extending the XGBoost with local interpretable model-agnostic explanations (LIME) in the XAI application. The explanations are quite useful in identifying faults and planning maintenance operations. The proposed XFDDS implementation, deployment and demonstration on multiple PV technologies was used to illustrate the capabilities. Extending XFDDS to include multiple faults and translating the approach to an edge are the future course of this investigation.

REFERENCES

- [1] T. Rajesh, K. Tamilselvan, A. Vijayalakshmi, C. N. Kumar, and K. A. Reddy, "Design and implementation of an automatic solar tracking system for a monocrystalline silicon material panel using mppt algorithm," *Materials Today: Proceedings*, 2020.
- [2] B. K. Karmakar and A. K. Pradhan, "Detection and classification of faults in solar pv array using thevenin equivalent resistance," *IEEE Journal of Photovoltaics*, vol. 10, no. 2, pp. 644–654, 2020.
- [3] Y. Zhao, R. Ball, J. Mosesian, J.-F. de Palma, and B. Lehman, "Graph-based semi-supervised learning for fault detection and classification in solar photovoltaic arrays," *IEEE Transactions on Power Electronics*, vol. 30, no. 5, pp. 2848–2858, 2014.
- [4] D. S. Pillai, F. Blaabjerg, and N. Rajasekar, "A comparative evaluation of advanced fault detection approaches for pv systems," *IEEE Journal of Photovoltaics*, vol. 9, no. 2, pp. 513–527, 2019.
- [5] B. Jin, D. Li, S. Srinivasan, S.-K. Ng, K. Poolla, and A. Sangiovanni-Vincentelli, "Detecting and diagnosing incipient building faults using uncertainty information from deep neural networks," in *2019 IEEE International Conference on Prognostics and Health Management (ICPHM)*. IEEE, 2019, pp. 1–8.
- [6] E. Garoudja, F. Harrou, Y. Sun, K. Kara, A. Chouder, and S. Silvestre, "Statistical fault detection in photovoltaic systems," *Solar Energy*, vol. 150, pp. 485–499, 2017.
- [7] A. Mellit, G. M. Tina, and S. A. Kalogirou, "Fault detection and diagnosis methods for photovoltaic systems: A review," *Renewable and Sustainable Energy Reviews*, vol. 91, pp. 1–17, 2018.
- [8] Z. Gao, C. Cecati, and S. X. Ding, "A survey of fault diagnosis and fault-tolerant techniques—part i: Fault diagnosis with model-based and signal-based approaches," *IEEE Transactions on Industrial Electronics*, vol. 62, no. 6, pp. 3757–3767, 2015.
- [9] Y. Chaibi, M. Malvoni, A. Chouder, M. Boussetta, and M. Salhi, "Simple and efficient approach to detect and diagnose electrical faults and partial shading in photovoltaic systems," *Energy Conversion and Management*, vol. 196, pp. 330–343, 2019.
- [10] S. Shongwe and M. Hanif, "Comparative analysis of different single-diode pv modeling methods," *IEEE Journal of photovoltaics*, vol. 5, no. 3, pp. 938–946, 2015.
- [11] F. Bradascchia, M. C. Cavalcanti, A. J. do Nascimento, E. A. da Silva, and G. M. de Souza Azevedo, "Parameter identification for pv modules based on an environment-dependent double-diode model," *IEEE Journal of Photovoltaics*, vol. 9, no. 5, pp. 1388–1397, 2019.
- [12] V. Khanna, B. Das, D. Bisht, P. Singh *et al.*, "A three diode model for industrial solar cells and estimation of solar cell parameters using pso algorithm," *Renewable Energy*, vol. 78, pp. 105–113, 2015.
- [13] M. H. Qais, H. M. Hasanien, and S. Alghuwainem, "Identification of electrical parameters for three-diode photovoltaic model using analytical and sunflower optimization algorithm," *Applied Energy*, vol. 250, pp. 109–117, 2019.
- [14] A. Triki-Lahiani, A. B.-B. Abdelghani, and I. Slama-Belkhdja, "Fault detection and monitoring systems for photovoltaic installations: A review," *Renewable and Sustainable Energy Reviews*, vol. 82, pp. 2680–2692, 2018.
- [15] M. Davarifar, A. Rabhi, A. El-Hajjaji, and M. Dahmane, "Real-time model base fault diagnosis of pv panels using statistical signal processing," in *2013 International Conference on Renewable Energy Research and Applications (ICRERA)*. IEEE, 2013, pp. 599–604.
- [16] S. Fadhel, C. Delpha, D. Diallo, I. Bahri, A. Migan, M. Trabelsi, and M. Mimouni, "Pv shading fault detection and classification based on iv curve using principal component analysis: Application to isolated pv system," *Solar Energy*, vol. 179, pp. 1–10, 2019.
- [17] M. H. Ali, A. Rabhi, A. El Hajjaji, and G. M. Tina, "Real time fault detection in photovoltaic systems," *Energy Procedia*, vol. 111, pp. 914–923, 2017.
- [18] L. Chen and X. Wang, "Adaptive fault localization in photovoltaic systems," *IEEE Transactions on Smart Grid*, vol. 9, no. 6, pp. 6752–6763, 2017.
- [19] Z. Yi and A. H. Etemadi, "Line-to-line fault detection for photovoltaic arrays based on multiresolution signal decomposition and two-stage support vector machine," *IEEE Transactions on Industrial Electronics*, vol. 64, no. 11, pp. 8546–8556, 2017.
- [20] —, "Fault detection for photovoltaic systems based on multi-resolution signal decomposition and fuzzy inference systems," *IEEE Transactions on Smart Grid*, vol. 8, no. 3, pp. 1274–1283, 2016.
- [21] Y. Zhao, T. Li, X. Zhang, and C. Zhang, "Artificial intelligence-based fault detection and diagnosis methods for building energy systems: Advantages, challenges and the future," *Renewable and Sustainable Energy Reviews*, vol. 109, pp. 85–101, 2019.
- [22] K. Dhibi, R. Fezai, M. Mansouri, M. Trabelsi, A. Kouadri, K. Bouzara, H. Nounou, and M. Nounou, "Reduced kernel random forest technique for fault detection and classification in grid-tied pv systems," *IEEE Journal of Photovoltaics*, 2020.
- [23] Y. Zhao, D. Li, T. Lu, Q. Lv, N. Gu, and L. Shang, "Collaborative fault detection for large-scale photovoltaic systems," *IEEE Transactions on Sustainable Energy*, 2020.
- [24] Y. Gan, Z. Chen, L. Wu, C. Long, S. Cheng, and P. Lin, "A novel fault diagnosis method for pv arrays using extreme gradient boosting classifier," 2019.
- [25] A. Ebrahimifakhar, A. Kabirikopaei, and D. Yuill, "Data-driven fault detection and diagnosis for packaged rooftop units using statistical machine learning classification methods," *Energy and Buildings*, vol. 225, p. 110318, 2020.
- [26] X.-H. Li, C. C. Cao, Y. Shi, W. Bai, H. Gao, L. Qiu, C. Wang, Y. Gao, S. Zhang, X. Xue *et al.*, "A survey of data-driven and knowledge-aware explainable ai," *IEEE Transactions on Knowledge and Data Engineering*, 2020.
- [27] S. Bramhall, H. Horn, M. Tieu, and N. Lohia, "Qlime-a quadratic local interpretable model-agnostic explanation approach," *SMU Data Science Review*, vol. 3, no. 1, p. 4, 2020.
- [28] A. Torres-Barrán, Á. Alonso, and J. R. Dorronsoro, "Regression tree ensembles for wind energy and solar radiation prediction," *Neurocomputing*, vol. 326, pp. 151–160, 2019.
- [29] V. J. Chin, Z. Salam, and K. Ishaque, "Cell modelling and model parameters estimation techniques for photovoltaic simulator application: A review," *Applied Energy*, vol. 154, pp. 500–519, 2015.
- [30] R. Sun, G. Wang, W. Zhang, L.-T. Hsu, and W. Y. Ochieng, "A gradient boosting decision tree based gps signal reception classification algorithm," *Applied Soft Computing*, vol. 86, p. 105942, 2020.
- [31] J. Fan, X. Wang, L. Wu, H. Zhou, F. Zhang, X. Yu, X. Lu, and Y. Xiang, "Comparison of support vector machine and extreme gradient boosting for predicting daily global solar radiation using temperature and precipitation in humid subtropical climates: A case study in china," *Energy Conversion and Management*, vol. 164, pp. 102–111, 2018.
- [32] N. Sapountzoglou, J. Lago, and B. Raison, "Fault diagnosis in low voltage smart distribution grids using gradient boosting trees," *Electric Power Systems Research*, vol. 182, p. 106254, 2020.